Floquet Fulde-Ferrell-Larkin-Ovchinnikov superfluids and Majorana fermions in a shaken fermionic optical lattice

Zhen Zheng, Chunlei Qu, Xubo Zou, and Chuanwei Zhang

Phys. Rev. A **91**, 063626 — Published 22 June 2015

DOI: 10.1103/PhysRevA.91.063626

Floquet FFLO superfluids and Majorana fermions in a shaken fermionic optical lattice

Zhen Zheng[1,2],* Chunlei Qu[1],* Xubo Zou[2], and Chuanwei Zhang[1]†
[1] *Department of Physics, The University of Texas at Dallas, Richardson, TX, 75080 USA*
[2] *Key Laboratory of Quantum Information, University of Science and Technology of China, Hefei, Anhui, 230026, People's Republic of China*

Fulde-Ferrell-Larkin-Ovchinnikov (FFLO) superfluids, Cooper pairings with finite momentum, and Majorana fermions (MFs), quasiparticles with non-Abelian exchange statistics, are two topics under intensive investigation in the past several decades, but unambiguous experimental evidences for them have not been found yet. Here we show that the recent experimentally realized shaken optical lattice provides a new pathway to realize FFLO superfluids and MFs. By tuning the shaking frequency and amplitude, various coupling between the s- and p-orbitals of the lattice (denoted as the pseudo-spins) can be generated. We show that the combination of the s- and p-band dispersion inversion, the engineered pseudo-spin coupling, and the on-site attractive interaction, naturally allows the observation of FFLO superfluids as well as MFs in different parameter regions.

PACS numbers: 03.75.Ss, 03.65.Vf, 74.20.Fg

I. INTRODUCTION

Optical lattices for ultra-cold atoms provide a generic platform for quantum simulation of various condensed matter phenomena because of their precise control of the system parameters and the lack of disorder [1]. In a static optical lattice, the Bloch bands are well separated by large energy gaps and usually only one orbital band plays a dominate role in the static and dynamical properties of ultra-cold atoms [2–10]. Recently, the experimentally realized shaken optical lattices opens a completely new avenue for studying the physics originating from the coupling between different orbital bands induced by the lattice shaking [11]. It was shown in experiment that the hybridization of s-band and p-band of a Bose-Einstein condensate (BEC) in a shaken lattice can cause a change of the energy dispersion from a parabolic to a double well structure, yielding a paramagnetic to ferromagnetic phase transition [11, 12, 60]. More generally, by varying the shaking parameters, various coupling between different Bloch bands can be engineered to implement artificial gauge fields for cold atoms, yielding exciting new exotic physics [13, 14], such as the recent experimental observation of topological Haldane model and the associated anomalous Hall effect [15].

In this article, we investigate new superfluid phases emerged from the coupling between the lowest two Bloch bands (s- and p-bands) in a shaken fermionic optical lattice. The s- and p-orbitals are denoted as two pseudo-spins, whose energy dispersions are inverted, in contrast to the same dispersion for usual spins. We show that such inverted band dispersions, together with on-site interactions between atoms on s- and p-bands, provide a natural way to realize the long-sought Fulde-Ferrell-Larkin-Ovchinnikov (FFLO) superfluids [16, 17]. Because of the inverted band dispersion, the FFLO state becomes the natural ground state of the system with a fixed FFLO momentum. Such inverted band induced FFLO pairing mechanism has not been well explored before and is completely different from the well-known Zeeman field [16–20] or asymmetric band dispersion [21–26] mechanisms, where the FFLO momentum is continuously tunable by the external Zeeman field.

When the shaking frequency and amplitude are tuned to certain regimes, the coupling between the two pseudo-spins may depend on the lattice quasi-momentum, analogous to the artificial spin-orbit coupling (SOC) [27–31]. However, because of the inverted band dispersions of two pseudo-spins, such coupling opens a band gap in the energy spectrum, instead of shifting band dispersions of different spins in the artificial SOC [27–31]. Therefore the system behaves like a topological insulator (TI) [32, 33] without interaction and supports topological edge states in the band gap. With many-body interaction, we show that there is a quantum phase transition from FFLO to BCS superfluids with the increasing SOC. The BCS superfluid is topological in most parameter regions and supports Majorana fermions (MFs) which are localized at the lattice boundaries [34, 35]. More interestingly, the topological BCS superfluids and MFs may utilize the conduction or valence bands of such a TI, instead of the edge states inside the band gap that are commonly used in previous TI-based schemes for MFs [36].

II. MODEL HAMILTONIAN

We first consider a degenerate spinless Fermi gas trapped in a three dimensional (3D) optical lattice. The shaking of the lattice is along the x direction [11], yielding a periodically modulating potential

$$V = V_x \cos^2[k_L x + f\cos(\omega t)] + \sum_{i=y,z} V_i \cos^2(k_L r_i) \quad (1)$$

* These authors contributed equally to this work
† chuanwei.zhang@utdallas.edu

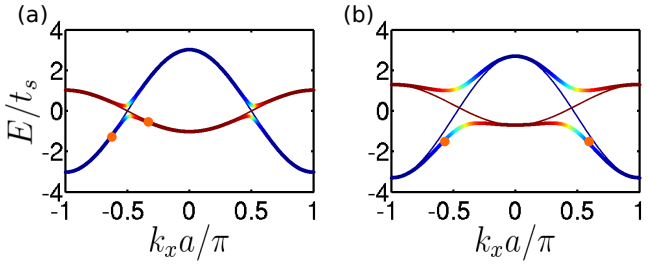

FIG. 1. (Color online) Single-particle band structure of the shaken lattice with (a) one-photon coupling $\Omega = 0.3t_s$; (b) two-photon coupling $\alpha = 1.0t_s$ and Zeeman field $h = 0.3t_s$. The band dispersions without coupling are shown as thin lines. The colors represent the band compositions of each momentum state. The orange filled circles denote the preferred Cooper pairings.

where V_i $(i = x, y, z)$ are the lattice depths, $k_L = \pi/a$, a is the lattice spacing that is set as the length unit. f and ω are the shaking amplitude and frequency, respectively. The energy dispersions of the static Bloch bands can be shifted by $n\hbar\omega$ (n is an arbitrary integer) due to the shaking, forming the new Floquet bands. The shaking also couples two close Floquet or static bands, leading to gaps in the energy spectrum, as illustrated in Fig. 1. Note that when the frequency $\hbar\omega$ is close to the energy gap between s- and p-orbital bands, the higher orbital bands involve only through a multi-photon process which contributes a very small correction. Therefore we here focus on the lowest s- and p-bands. Because the shaking is along the x direction, only the p_x-band can be coupled with the s-band and atoms stay at the s-band along the other two directions. When $\hbar\omega$ is tuned close to the band gap (Δ_g) of the static lattices, the s-orbital state can absorb an energy of $\hbar\omega$ and couple with the p_x-orbital state. Such "one-photon process" coupling strength is denoted by Ω, which can be approximated as a constant [61]. If $2\hbar\omega \sim \Delta_g$, the s-orbital band is shifted upward by two photon energy $2\hbar\omega$ to couple with the p_x-band. In this "two-photon process", by properly tuning the frequency and amplitude of the shaking, the dominate term is the coupling between s- and p_x-orbital states of the nearest neighboring sites which simulates a SOC [61].

For a deep shaken lattice, the system can be well described by an effective two-band model. In the basis of $(\psi_s(\boldsymbol{k}), \psi_{p_x}(\boldsymbol{k}))^T$, the single-particle Hamiltonian in momentum space reads

$$\mathcal{H}_0(\boldsymbol{k}) = \begin{pmatrix} \epsilon_s(\boldsymbol{k}) + h & \Pi_{\boldsymbol{k}} \\ \Pi_{\boldsymbol{k}} & \epsilon_p(\boldsymbol{k}) - h \end{pmatrix} \tag{2}$$

under the tight-binding approximation. Here $\epsilon_s(\boldsymbol{k}) = -t_s \cos(k_x a) - t_s^{\perp} [\cos(k_y a) + \cos(k_z a)] - \mu$ and $\epsilon_p(\boldsymbol{k}) = t_p \cos(k_x a) - t_s^{\perp} [\cos(k_y a) + \cos(k_z a)] - \mu$, where t_s and t_p are the nearest neighbor tunneling amplitudes for an atom in s-orbital and p-orbital states along the x direction, and $t_s^{\perp}$ is the tunneling amplitudes along the y and z directions. For one-photon dominated processes, $\Pi_{\boldsymbol{k}} = \Omega$ is the $\boldsymbol{k}$-independent coupling strength between the two orbital states. For two-photon dominated processes, $\Pi_{\boldsymbol{k}} = \alpha \sin(k_x a)$ is the $\boldsymbol{k}$-dependent coupling strength which simulates the SOC. μ is the chemical potential, h is the off-resonance detuning determined by the difference of the shaking frequency and the band gap. Fig. 1 illustrates the effective band structures of the one-photon and two-photon processes. With a finite coupling Ω or $\alpha \sin(k_x a)$, two bands are hybridized around the crossing points, and thus yield an energy gap.

We consider on-site attractive interaction between atoms on different orbital bands. The renormalization of the periodic driving on the on-site interaction is small and thus ignored in the following calculations (See Appendix C 2). In the momentum space, the interaction Hamiltonian can be written as $\mathcal{H}_I = -U \sum \psi_s^{\dagger}(\boldsymbol{k}_1)\psi_{p_x}^{\dagger}(\boldsymbol{k}_2)\psi_{p_x}(\boldsymbol{k}_3)\psi_s(\boldsymbol{k}_4)$, where $\boldsymbol{k}_1 + \boldsymbol{k}_2 = \boldsymbol{k}_3 + \boldsymbol{k}_4$ due to the momentum conservation in the two-body scattering processes, $U > 0$ is the interaction strength.

As the first step approach for a qualitative understanding of the interacting Fermi gas in a shaken optical lattice, we consider the mean-field approximation and assume a single-plane-wave FF-type order parameter, *i.e.*, $\Delta = U\langle\psi_{p_x}(\frac{\boldsymbol{Q}}{2} - \boldsymbol{k})\psi_s(\frac{\boldsymbol{Q}}{2} + \boldsymbol{k})\rangle$, where $\mathbf{Q} = (Q, 0, 0)$ is the FF vector along the x direction. $\boldsymbol{Q} = 0$ corresponds to a conventional BCS superfluid. The dynamics of the system is governed by the Bogliubov-de Gennes (BdG) Hamiltonian,

$$\mathcal{H}_{\mathrm{BdG}}(\boldsymbol{k}) = \begin{pmatrix} \mathcal{H}_0(\frac{\boldsymbol{Q}}{2} + \boldsymbol{k}) & \Delta \\ \Delta^* & -\sigma_y \mathcal{H}_0^*(\frac{\boldsymbol{Q}}{2} - \boldsymbol{k})\sigma_y \end{pmatrix}, \tag{3}$$

in the Nambu-Gorkov spinor basis $[\psi_s(\frac{\boldsymbol{Q}}{2} + \boldsymbol{k}), \psi_{p_x}(\frac{\boldsymbol{Q}}{2} + \boldsymbol{k}), \psi_{p_x}^{\dagger}(\frac{\boldsymbol{Q}}{2} - \boldsymbol{k}), -\psi_s^{\dagger}(\frac{\boldsymbol{Q}}{2} - \boldsymbol{k})]^T$. The gap and momentum equations are solved by minimizing the thermodynamic potential to obtain Δ and Q, through which we determine different phases (See Appendix A 1). When $\Delta \neq 0$ and $Q \neq 0$, the system is in a FFLO phase. When $\Delta \neq 0$, $Q = 0$, the system is in a BCS phase. Otherwise, the system is a normal gas or a band insulator.

III. PHASE DIAGRAMS IN 3D LATTICES

In Fig. 2 we plot the phase diagrams for resonant one-photon (Fig. 2(a)) and two-photon processes (Fig. 2(b)) with $t_p = 3t_s$, $t_s^{\perp} = t_s$, respectively. The phase diagram is similar for quasi-2D and quasi-1D systems with $t_s^{\perp} \to 0$ (See Appendix D). The system favors FFLO states in a large parameter regime with a finite momentum along the shaking direction $Q_x = \pm\pi/a$. Here the FFLO pairing originates from the intrinsic band dispersion inversion between s- and p_x-bands, which suppresses the conventional BCS pairing. This can be further understood through a coordinate transformation $k_x' \to k_x' \pm \pi/a$ for the p_x-band dispersion to remove the band inversion. In the system without the band inversion, we expect a conventional BCS superfluids between k_x and $-k_x$, leading

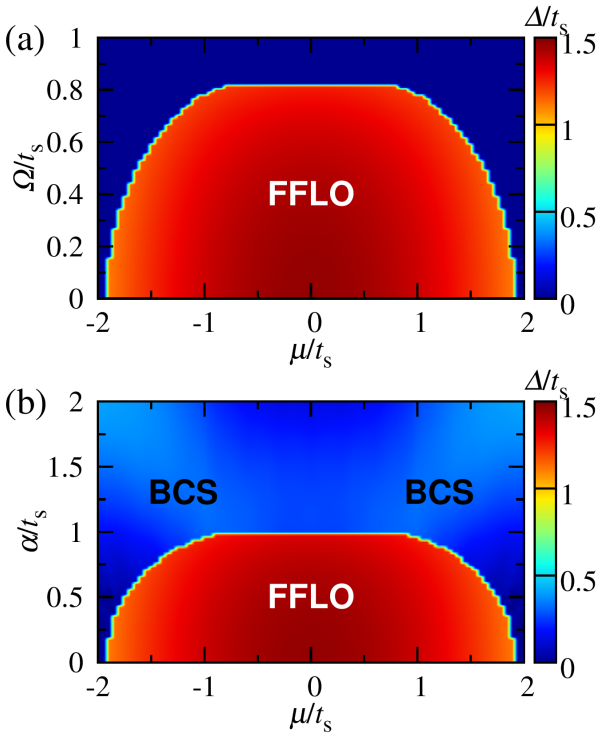

FIG. 2. (Color online) Phase diagram of a 3D shaken optical lattice with (a) one-photon coupling Ω or (b) two-photon coupling α. Other parameters $U = 4.0t_s$, $h = 0.0$, $t_p = 3t_s$, $t_s^\perp = t_s$.

to $k_x' \pm \pi/a = -k_x$. Therefore the preferred pairings in the shaken lattice are between two spins with momenta of k_x and $k_x' = \pm\pi/a - k_x$, and the FFLO momentum is $Q_x = \pm\pi/a$ (See Appendix B). The analysis still applies in the presence of small SOC and Zeeman fields. Note that such inverted band induced FFLO pairing with a fixed $\mathbf{Q}$ has not been well explored before and is completely different from the well-known Zeeman field [16–20] or asymmetric band dispersion [21, 22] mechanisms.

For larger Ω, the gap between two hybrid bands is very large, thus a band insulator phase appears near the half filling. Each of the hybrid band polarizes to one spin state for a large Ω, leading to vanishing Cooper pairing. In the presence of small SOC $\sim \alpha\sin(k_x a)$, the system still favors the FFLO superfluid. However, the SOC leads to different wavefunctions at k_x and $-k_x$, leading to the BCS pairing, as observed in Fig. 2(b) for larger SOC.

IV. TOPOLOGICAL PHASE AND MAJORANA FERMIONS IN 1D LATTICES

Hereafter we focus on possible topological phases induced by the SOC in the two-photon process. It is well known that there is no topological phases in a 3D system with such 1D SOC. To reach the topological phase that may support topological excitations such as MFs, we need to consider a quasi-1D system with small or vanishing transverse tunneling $t_s^\perp$. We first present the results for $t_s^\perp = 0$ for simplicity, and then discuss how a small $t_s^\perp$ modifies the phase diagram and the topological phases. In Fig. 3, we plot the phase diagrams in the presence of a Zeeman field h for two different SOC strengths, where a new phase, topological BCS (t-BCS) superfluids that host MFs, emerges in a large parameter regime. The transition from BCS to t-BCS is characterized by the bulk quasiparticle excitation spectrum closing and reopening at $k_x = 0$ (and $k_x = \pm\pi/a$) and can be understood from the symmetry of the BdG Hamiltonian. The BdG Hamiltonian (3) satisfies the particle-hole symmetry $\Xi\mathcal{H}_{\rm BdG}(k_x)\Xi^{-1} = -\mathcal{H}_{\rm BdG}(-k_x)$, where $\Xi = \Lambda\mathcal{K}$, $\Lambda = \sigma_x\tau_z$ and $\mathcal{K}$ is the complex conjugate operator. For a BCS superfluid ($Q_x = 0$), if $t_p = t_s$, it also respects a time-reversal-like symmetry $\mathcal{T}\mathcal{H}_{\rm BdG}(k_x)\mathcal{T}^{-1} = \mathcal{H}_{\rm BdG}(-k_x)$, where $\mathcal{T} = \sigma_z\tau_0\mathcal{K}$. This topological BCS superfluid belongs to the BDI symmetry class characterized by a $\mathbb{Z}$ invariant and MFs can be found at the boundary of the superfluids [38–40]. If $t_p \neq t_s$, it belongs to the more generalized D symmetry class characterized by a $\mathbb{Z}_2$ invariant. The topological BCS phase region can be determined by the Pfaffian sign of the skew matrix $\Gamma(k_x) = H_{\rm BdG}(k_x)\Lambda$, yielding $\text{sign}[\text{Pf}(\Gamma(0)) \times \text{Pf}(\Gamma(\pi))] = -1$, which has an explicit form

$$[(t_+ - h)^2 - \Delta^2 - (\mu + t_-)^2]\times [(t_+ + h)^2 - \Delta^2 - (\mu - t_-)^2] < 0\ , \quad (4)$$

where $t_+ = (t_s + t_p)/2$, $t_- = (t_s - t_p)/2$.

Because $t_p \neq t_s$, the phase diagrams are not symmetric about $h = 0$ or $\mu = 0$ as shown in Fig. 3. However, the system is symmetric with the transformation $h \to -h$ and $\mu \to -\mu$. This is in stark contrast to conventional systems (with two pseudo-spins both in s-bands), where the phase diagrams are symmetric with respect to either $h = 0$ or $\mu = 0$ and the Zeeman field must be larger than a critical value for the appearance of t-BCS phase.

From Fig. 3, we see the FFLO superfluid dominates for small SOC and the region of t-BCS superfluids does not change much when the strength of SOC is increased. There exists an insulator block with $\Delta = 0$ near $\mu = 0$ surrounded by the superfluid phase in Fig. 3(b). Note that for a 1D non-interacting system with $t_s^\perp = 0$ and $t_p = t_s$, the single particle Hamiltonian $\mathcal{H}_0$ breaks the time reversal symmetry but preserves a chiral symmetry $\sigma_y\mathcal{H}_0(k_x)\sigma_y = -\mathcal{H}_0(k_x)$, which realizes an AIII class TI characterized by a $\mathbb{Z}$ topological invariant [38, 39]. In the topological phase, there are a pair of in-gap topological states on the system boundaries [41–43]. When $t_p \neq t_s$, there will be an additional kinetic energy term, which does not change the phase transition and topological properties of the system [44, 45]. With the interaction tuned on in Fig. 3(a,b), the system evolves into a topological superfluids with finite BCS order parameters. The original edge states of the topological insulator are now replaced by the zero energy Majorana boundary

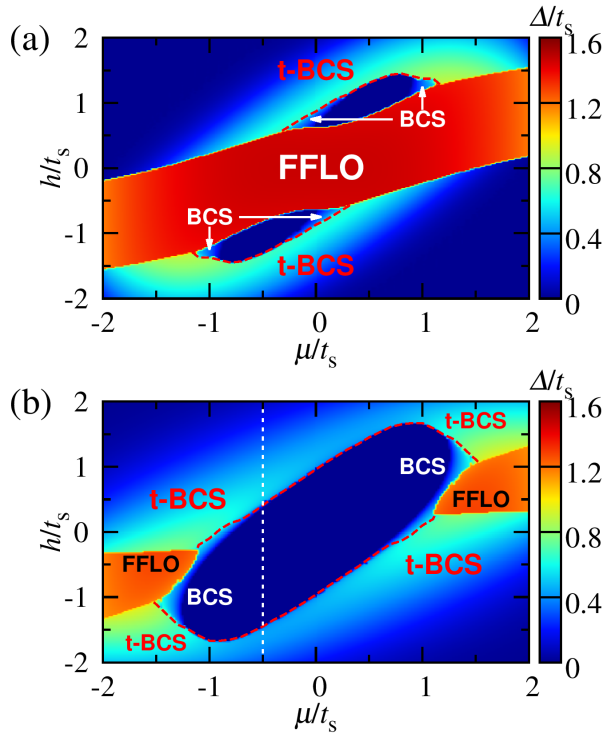

FIG. 3. (Color online) Phase diagram of the 1D shaken optical lattice with two-photon coupling. (a) $\alpha = 0.7t_s$; (b) $\alpha = 1.4t_s$. The red dashed lines are the boundary between BCS/insulator and t-BCS superfluids. $U = 4.0t_s$, $t_p = 3t_s$, $\Omega = 0.0$.

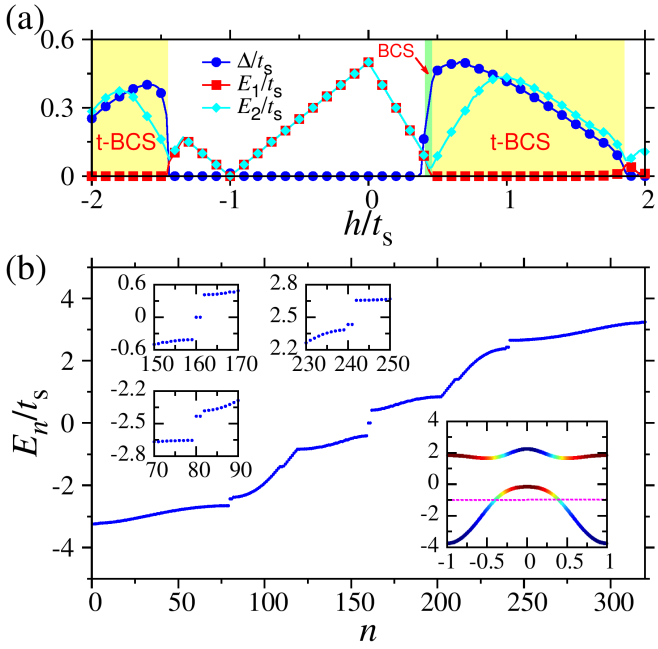

FIG. 4. (Color online) Majorana fermions in a shaken optical lattice. (a) The order parameter Δ (Blue circles) and the lowest two quasi-particle excitation energies E_1 (red squares), E_2 (cyan diamonds) as a function of Zeeman field h. $\alpha = 1.4t_s$. Unlabeled white regions correspond to either normal gas or insulator phase. Other parameters are $\mu = -0.5t_s$, $U = 4.0t_s$, $\Omega = 0.0$, $t_p = 3t_s$. (b) BdG quasi-particle excitation energies for $\alpha = 1.4t_s$, $\mu = -0.7t_s$, $h = 0.8t_s$. There are three pairs of sub-gap states all localized on the boundaries.

states [41] when the chemical potential is in the band gap, similar as previous TI based MF scheme using edge states [36]. More interestingly, when the chemical potential cuts only one of the conduction or valance bands, we find the coexistence of the edge states from the topological insulator and the zero energy Majorana edge states from the topological superconductor.

The above momentum space analysis is further confirmed by self-consistently solving the BdG Hamiltonian in the real space. In Fig. 4(a) we plot the average value of the order parameter Δ and the lowest two quasi-particle excitation energies E_1 and E_2 as a function of the Zeeman field h. In consistent with the white dashed line in Fig. 3(b), there is a phase transition from insulator phase to trivial BEC superfluids and then to a topological BCS superfluids at $h \approx 0.45t_s$. The momentum of FFLO Cooper pairs in real space is either FF or LO types, both have the same ground state energies as that in momentum space. In the topological phase, the zero energy MFs are protected by a finite mini-gap E_2. In Fig. 4(b) we plot of the BdG quasi-particle excitation energies for $\alpha = 1.4t_s$. The inset shows the quasi-particle excitation spectrum with zero energy degenerate MF states and the single particle band structure where the chemical potential cuts a single conduction band. The zero energy MF modes are localized on the system boundaries. As mentioned in the above, for $\mu \neq 0$ and when the chemical potential cuts either of the two bands, we may find another two pairs of sub-gap edge states with finite energies which are induced by the topological insulator and coexist with the MFs edge states from the topological superconductor (See Appendix E for the real space wave functions of these coexist edge states).

The interaction strength U can be easily tuned in cold atom experiments which provides a way to study the crossover from the BCS superfluids with weak attractive interaction to the Bose-Einstein condensation (BEC) of strongly bounded molecules. BCS-BEC crossover has been widely studied in ultracold Fermi gases in various free space and optical lattice systems [46, 47]. In Fig. 5 we plot the phase diagrams in h-U plane for a two-photon coupling process with different strengths of SOC (a) $\alpha = 0.7t_s$ (b) $\alpha = 1.4t_s$ for a certain value of chemical potential. In consistent with Fig. 3 (a)(b) of the main text we see FFLO superfluid phase dominates for small SOC and small Zeeman field, and BCS phase dominates for large Zeeman field or large SOC. The topological phase appears when the strength of the Zeeman field exceeds a critical value for a medium value of interaction strength U and tends to disappear at the BEC side. Because SOC leads to an energy gap near half filling, the band insulator occupies a larger parameter region when

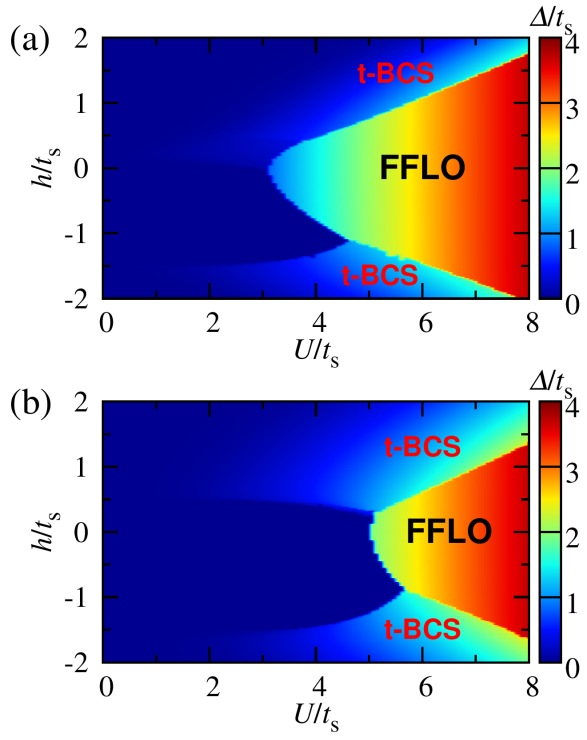

FIG. 5. (Color online) BCS-BEC crossover. Color plots of the order parameter in the $h-U$ plane for small SOC (a) $\alpha = 0.7t_s$ and large SOC (b) $\alpha = 1.4t_s$. The chemical potential is taken as $\mu = -0.5t_s$, and $\Omega = 0.0$, $t_p = 3t_s$.

SOC coupling strength is increased in the BCS side.

More generally, we can consider quasi-1D atom tubes generated by optical lattices in a 3D system with weak tunnelings along the transverse directions for the search of MFs. The weak transverse tunneling can strongly suppress the quantum fluctuations along the 1D tubes, similar as that in high temperature cuprate superconductors. Consider a periodic boundary condition along the transverse directions, the weak tunneling simply shifts the chemical potential of the 1D gas at most by $4t_s^{\perp}$ in Eq. (4). As long as the shifted chemical potential still stays inside the topological BCS region, we expect the MFs exist along the tube edges. Similar issue for MFs has been widely discussed in spin-orbit coupled quantum wires (nanowire or cold atom tube arrays [48–50]) and our calculations show that the same conclusion still holds for the shaken optical lattices.

V. EXPERIMENTAL REALIZATION

Fermions confined in 3D or quasi-1D optical lattices have been realized in experiments and the Hamiltonian (2) can be generated by shaking [11] or other means [51]. For a spinless Fermi gas, the s-wave scattering interactions between same orbital states are usually prohibited by the Pauli exclusion principle, and the interactions between different orbital states are usually very small. However, the strong on-site attractive interactions can be engineered using different methods (See Appendix C 1), such as the use of the dipole-dipole interaction between dipolar atoms [52]. Recently, dipolar BEC and degenerate dipolar Fermi gases have been observed in experiments [53–56]. When the dipoles are aligned along the 1D direction (i.e., head to head), the dipole interaction between atoms ($\sim 1/r^3$) is attractive. The long rang dipole interaction can lead to attractive on-site interaction between atoms with different orbital states at the same lattice site, which is much larger than the interaction between atoms at nearest neighboring sites. The on-site interaction can be tuned by the lattice confinement along the transverse directions. The FFLO pairing may be observed by sound speed measurement [57] with a fixed pairing momentum. MFs may be observed using the radio-frequency spectroscopy [58].

VI. DISCUSSIONS

The shaking lattice scheme is very different and has many advantages over widely studied Zeeman field or SOC schemes for generating FFLO states [16–22]. Here the FFLO pairing originates from the inversion of two pseudospin band dispersions, leading to a fixed pairing momentum at $\pm\pi/a$, which is completely different from the Fermi surface mismatch mechanism induced by the Zeeman field or the asymmetric Fermi surface mechanism induced by a combination of SOC and Zeeman field, where the FFLO momentum is determined by the system parameters [16–22]. At a finite temperature, the thermodynamic fluctuations suppress the superfluid phase. However, the FFLO pairing always exists in the superfluid phase for the inverted bands. Furthermore, the external Zeeman field in the SOC system must exceed a nonzero critical value for the topological phase and MFs. The Zeeman field strongly suppresses the order parameter, therefore it is hard to observe FFLO states and the topological BCS phase only occurs in a small parameter region in previous SOC schemes. In our shaking lattice scheme, no Zeeman field is necessary. The FFLO state is the natural ground state and almost all BCS phases are topological. Our scheme resembles to the topological insulator (which also has band inversion) based MF scheme, instead of the SOC one. The presence of the harmonic trap leads to a spatially dependent chemical potential, where different superfluid phases may be observed in different radius of the trapped system [59]. Finally, all lasers are far-detuned with little heating from lasers, in contrast to the near-resonant Raman lasers in the SOC scheme.

ACKNOWLEDGMENTS

We thank Yong Xu, Chris Hamner and Peter Engels for helpful discussions. C. Qu and C. Zhang are supported by ARO (W911NF-12-1-0334) and AFOSR (FA9550-11-1-0313). Z. Zheng and X. Zou are supported by National Natural Science Foundation of China (Grant No. 11074244 and Grant No. 11274295), and National 973 Fundamental Research Program (2011cba00200).

Appendix A: Mean-field model

1. In the momentum space

Consider the order parameter $\Delta(\boldsymbol{r}) = U\langle\psi_p\psi_s\rangle = \Delta e^{i\boldsymbol{Q}\cdot\boldsymbol{r}}$, where $\boldsymbol{Q}$ is the pairing momentum, the thermodynamical potential is given by

$$\Omega = \frac{1}{2}\sum_{\boldsymbol{k}}\Big(\epsilon_s(\boldsymbol{Q}/2-\boldsymbol{k}) + \epsilon_p(\boldsymbol{Q}/2-\boldsymbol{k})\Big) + \sum_{\boldsymbol{k}\lambda}\Theta\Big(-E_\lambda(\boldsymbol{k})\Big)E_\lambda(\boldsymbol{k}) + \frac{|\Delta|^2}{U}\ , \qquad \text{(A1)}$$

where $\Theta(x)$ is the Heaviside function representing the Fermi distribution at zero temperature. $E_\lambda(\boldsymbol{k})(\lambda = 1,\cdots,4)$ are the four eigenvalues of the BdG Hamiltonian $\mathcal{H}_{\rm BdG}(\boldsymbol{k})$. The order parameter Δ and momentum $\boldsymbol{Q}$ are hence given by self-consistently solving the saddle equations of the thermodynamical potential Ω:

$$\frac{\partial\Omega}{\partial\Delta} = 0\ , \qquad \frac{\partial\Omega}{\partial\boldsymbol{Q}} = 0\ . \qquad \text{(A2)}$$

2. In the real space

In the real space the tight-binding Hamiltonian is written as

$$H_{\rm TB} = H_0 + H_{\rm Z} + H_\alpha + V_{\rm int}\ , \qquad \text{(A3)}$$

where

$$H_0 = \sum_{\langle i,j\rangle}\Big(-t_s c_i^\dagger c_j + t_p c_i^\dagger c_j\Big) - \mu\sum_{i,\sigma=s,p} n_{i\sigma}, \qquad \text{(A4)}$$

$$H_{\rm Z} = -h_z\sum_i (n_{is} - n_{ip}), \qquad \text{(A5)}$$

$$H_\alpha = \frac{\alpha}{2}\sum_i (c_{i-1p}^\dagger c_{is} - c_{i+1p}^\dagger c_{is} + \text{H.C.}), \qquad \text{(A6)}$$

$$V_{\rm int} = -U\sum_i n_{is}n_{ip}, \qquad \text{(A7)}$$

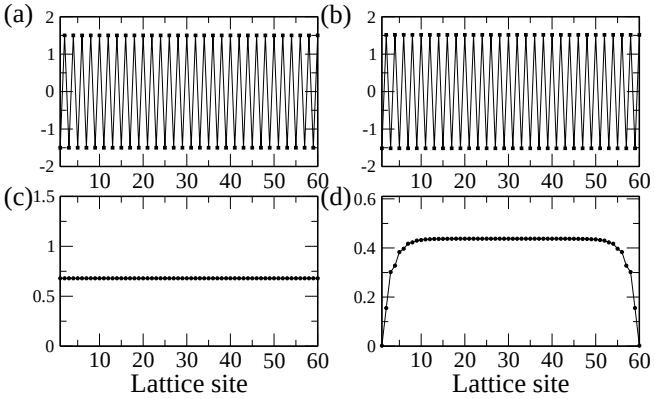

FIG. 6. Self-consistently obtained order parameter in real space. (a) $\Omega = 0.3t_{\rm s}$, $\mu = 0.5t_{\rm s}$, the system is in FFLO phase; (b) $\alpha = 0.3t_{\rm s}$, $\mu = 0.5t_{\rm s}$, the system is in FFLO phase; (c) $\alpha = 1.2t_{\rm s}$, $\mu = 1.2t_{\rm s}$, the system is in trivial BCS phase; (d) $\alpha = 1.2t_{\rm s}$, $\mu = 1.2t_{\rm s}$, $h = -0.5t_{\rm s}$, the system is in topological BCS phase where we adopt open boundary condition for the appearance of MFs. Other parameters: $U = 4.0t_{\rm s}$, $t_{\rm p} = 3t_{\rm s}$.

The mean field order parameters

$$\Delta_i = U\langle c_{ip}c_{is}\rangle. \qquad \text{(A8)}$$

We have defined c_i and $c_i^\dagger$ as the particle annihilation and creation operator on site i and the particle number operator $n_{i\sigma=s,p} = c_{i\sigma}^\dagger c_{i\sigma}$.

Our numerical calculations are done in both momentum space and real space, which agrees very well with each other. In Fig. 6, we present the order parameter profiles in various phases from real space calculations.

Appendix B: Mechanism of FFLO pairing

To demonstrate why the system favors FFLO pairing with a finite momentum $Q = \pm\pi/a$ along the SOC direction, we start with the most simplest case, i.e., with vanishing α, h and μ and consider only the 1D system. If we choose the Nambu-Gorkov spinor $\Psi = \Big(\psi_s(k_x), \psi_p(k'_x), \psi_p^\dagger(k'_x), \psi_s^\dagger(k_x)\Big)^T$, and introduce a general pairing order parameter $\Delta = U\langle\psi_p\psi_s\rangle$ the BdG Hamiltonian $\mathcal{H}_{\rm BdG}(k_x)$ is rewritten as

$$\mathcal{H}_{\rm BdG}(k_x, k'_x) = \begin{pmatrix} T(k_x,k'_x) & \Delta \\ \Delta^* & -\sigma_y T(k_x,k'_x)\sigma_y \end{pmatrix}\ , \qquad \text{(B1)}$$

where $T(k_x, k'_x) = \text{diag}[-t_s\cos(k_x a), t_p\cos(k'_x a)]$. When transferred to a new spinor basis $\Psi' = \Big(\psi_s(k_x), \psi_p(k'_x - \frac{\pi}{a}), \psi_p^\dagger(k'_x - \frac{\pi}{a}), \psi_s^\dagger(k_x)\Big)^T$ through a unitary transformation $\Psi = U\Psi'$ with $U = \text{diag}(1, e^{i\pi x/a}, e^{-i\pi x/a}, 1)$, we

get

$$\mathcal{H}'_{\rm BdG}(k_x,k_x'^{\dagger}) = U\mathcal{H}_{\rm BdG}(k_x,k_x')U^{\dagger} \quad \text{(B2)}$$

$$= \begin{pmatrix} T(k_x,k_x'-\frac{\pi}{a}) & \widetilde{\Delta} \\ \widetilde{\Delta}^* & -\sigma_y T(k_x,k_x'-\frac{\pi}{a})\sigma_y \end{pmatrix} . \quad \text{(B3)}$$

Here $\widetilde{\Delta} = \langle\psi_p(k_x'-\pi/a)\psi_s(k_x)\rangle$. Notice that $T(k_x,k_x'-\frac{\pi}{a}) = \mathrm{diag}[-t_s\cos(k_x a),-t_p\cos(k_x' a)]$ correspond to the conventional bands which are known to favor a BCS pairing in this new basis. It leads to $k_x = -(\pm\pi/a + k_x')$ and hence $k_x + k_x' = \pm\pi/a$. As a result the pairing momentum should be fixed to $\pm\pi/a$.

Appendix C: On-site attractive interaction

1. Generation of on-site interactions

For a three dimensional optical lattice, each well can be expanded around its center as a harmonic oscillator potential

$$V(\boldsymbol{r}) = \frac{1}{2}m(\omega_x^2x^2+\omega_y^2y^2+\omega_z^2z^2) , \quad \text{(C1)}$$

where $\boldsymbol{r} = (x,y,z)$. We focus on the on-site interaction of the lowest two orbital states, for instance s- and p_x-orbital states, and assume an s-orbital state along both y- and z-axes. The wave functions for s- and p_x-orbital states in this harmonic potential are given by

$$\psi_s(\boldsymbol{r}) = \Big(\frac{m}{\pi\hbar}\Big)^{\frac{3}{4}}\omega_x^{\frac{1}{4}}\omega_y^{\frac{1}{4}}\omega_z^{\frac{1}{4}}e^{-m(\omega_x x^2+\omega_y y^2+\omega_z z^2)/2\hbar} ,$$

$$\psi_p(\boldsymbol{r}) = \sqrt{2\pi}\Big(\frac{m}{\pi\hbar}\Big)^{\frac{5}{4}}\omega_x^{\frac{3}{4}}\omega_y^{\frac{1}{4}}\omega_z^{\frac{1}{4}}xe^{-m(\omega_x x^2+\omega_y y^2+\omega_z z^2)/2\hbar} .$$

In the Hartree-Fock approximation, the on-site interaction can be evaluated as,

$$\begin{aligned} -U &= \int d^3r_1d^3r_2\ V(\boldsymbol{r}_1-\boldsymbol{r}_2)\Big[|\psi_s(\boldsymbol{r}_1)\psi_p(\boldsymbol{r}_2)|^2 \\ &\quad -\psi_s^*(\boldsymbol{r}_1)\psi_p^*(\boldsymbol{r}_2)\psi_s(\boldsymbol{r}_2)\psi_p(\boldsymbol{r}_1)\Big] \\ &= \frac{2m^4}{\pi^3\hbar^4}\omega_x^2\omega_y\omega_z\int d^3Rd^3r\ V(\boldsymbol{r})r_x(r_x/2-R_x) \\ &\quad \exp\Big[-\frac{m}{\hbar}\sum_{i=x,y,z}\omega_i(R_i^2+r_i^2/4)\Big] , \end{aligned} \quad \text{(C2)}$$

where we have introduced $\boldsymbol{r} = \boldsymbol{r}_1-\boldsymbol{r}_2$ and $\boldsymbol{R} = (\boldsymbol{r}_1+\boldsymbol{r}_2)/2$. For simplicity, we assume $\omega_y = \omega_z = \omega$ in following calculations. For the fermionic atomic gas with a dipole moment $\boldsymbol{M}$, the anisotropic interaction is expressed as

$$V(\boldsymbol{r}) = \frac{\mu_0|\boldsymbol{M}|^2}{4\pi}\frac{[1-3(\hat{M}\cdot\hat{r})]^2}{r^3} , \quad \text{(C3)}$$

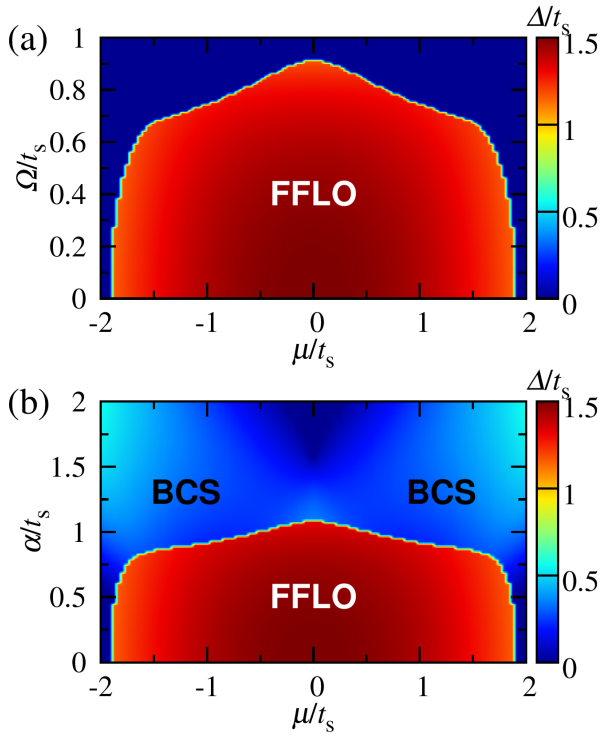

FIG. 7. (Color online) Phase diagram of the 2D shaken optical lattice with (a) one-photon coupling Ω and (b) two-photon coupling α . The color describes the magnitude of the order parameter Δ in unit of t_s. Other parameters $U = 4.0t_s$, $h = 0.0$, $t_p = 3t_s$, $t_s^{\perp} = t_s$.

where $\hat{M} = \boldsymbol{M}/|\boldsymbol{M}|$ and $\hat{r} = \boldsymbol{r}/|\boldsymbol{r}|$. Substituting it into the on-site interaction expression Eq. (C2), we get

$$-U = 2\Big(\frac{m\omega}{\pi\hbar}\Big)^{\frac{3}{2}}\frac{\mu_0|\boldsymbol{M}|^2}{4\pi}\ \times F(\frac{\omega_x}{\omega}) \quad \text{(C4)}$$

where

$$F(\frac{\omega_x}{\omega}) = \int_0^{2\pi}d\theta\int_0^{\pi}d\phi\frac{(\frac{\omega_x}{\omega})^{\frac{3}{2}}\cos^2\theta\sin^3\phi\ [1-3(\hat{M}\cdot\hat{r})]^2}{(\frac{\omega_x}{\omega}\cos^2\theta+\sin^2\theta)\sin^2\phi+\cos^2\phi} .$$

In a real experiment, we can use fermionic atoms of ^{167}Er with $M = 7\mu_B$. The optical lattice can be created by laser beams with the wavelength $\lambda \approx 600nm$. The recoil energy of such an optical lattice is $E_R = h^2/2m\lambda = 157nK$. For a typical tunneling energy $t_s \approx 0.36E_R \approx 55nK$. The on-site interaction $U \approx 224nK$ when $\omega_x/\omega \approx 0.3$ hence $U \approx 4t_s$ adopted in our paper can be obtained in real experiments.

2. On-site interactions in the rotating frame

The time-dependent lattice potential induces the couplings between different orbital bands and may also modify the diagonal intra-orbital terms to be time-dependent. To get the effective static Hamiltonian, we usually change

to a rotating frame to eliminate the diagonal time-dependent terms which may modify the interactions at the same time. In this section, we study the validity of a on-site s-wave interaction approximation that adopted in the main text.

Similar as reference [60, 61], the field operator $\Psi(x)$ for the time-dependent single-particle Hamiltonian

$$H_0(t) = \int dx \Psi^\dagger(x) \mathcal{H}_0(t) \Psi(x) \tag{C5}$$

$$\mathcal{H}_0(t) = -\frac{\hbar^2}{2m}\frac{\partial^2}{\partial x^2} + V\cos^2[k_L x + f\cos(\omega t)] \tag{C6}$$

can be expanded by the Wannier functions, $\Psi(x) = \sum_{\nu,i} W_\nu(x - x_i)c_{\nu i}$ $(\nu = s, p)$, of the static lattice Hamiltonian

$$H_s = -\frac{\hbar^2}{2m}\frac{\partial^2}{\partial x^2} + \frac{V}{2}J_0(f)\cos(2k_L x) \ . \tag{C7}$$

Therefore $H_0(t)$ is expressed as

$$H_0(t) = \sum_{ij}\Big(- t_s c^\dagger_{\nu i}c_{\nu j} + t_p c^\dagger_{\nu i}c_{\nu j} + H.c.\Big) + \sum_{\mu\nu,ij}\widetilde{\Omega}^{\mu\nu}_{ij}(t)c^\dagger_{\mu i}c_{\nu j} \ . \tag{C8}$$

For the one-photon and two-photon processes, we have

$$\widetilde{\Omega}^{\mu\nu}_{ij}(t) = \hat{\Omega}^{\mu\nu}_{ij}e^{i\omega t} \ , \quad \hat{\Omega}^{\mu\nu}_{ij} = (-1)^l J_{2l-1}(f)\frac{V}{2}\int dx \ W^*_\mu(x - x_i)\sin(2k_L x)W_\nu(x - x_j) \ . \tag{C9}$$

$$\widetilde{\Omega}^{\mu\nu}_{ij}(t) = \hat{\alpha}^{\mu\nu}_{ij}e^{i2\omega t} \ , \quad \hat{\alpha}^{\mu\nu}_{ij} = (-1)^l J_{2l}(f) \times \frac{V}{2}\int dx \ W^*_\mu(x - x_i)\cos(2k_L x)W_\nu(x - x_j) \ , \tag{C10}$$

respectively. Here $l = 1, 2, \cdots$ and $J_l(x)$ is the l-th order Bessel functions. We focus on couplings between two atoms in the same site or between two nearest-neighbouring sites. Due to the parity of Wannier functions and trigonometric functions, we know $\hat{\Omega}^{ss}_{ii} = \hat{\Omega}^{pp}_{ii} = 0$ and $\hat{\alpha}^{sp}_{ii} = \hat{\alpha}^{ps}_{ii} = 0$. Therefore for the one-photon process, there is no rotation-frame modification to the onsite interaction, while for the two-photon process we need to consider it.

In the rotating transformation under

$$U(t) = \exp\Big(\frac{i}{\hbar}\int_0^t dt' {}^{i2\omega t'}\sum_{\nu,mn}\hat{\alpha}^{\nu\nu}_{mn}c^\dagger_{\nu m}c_{\nu n}\Big) = \exp\Big(\frac{e^{i2\omega t} - 1}{2\hbar\omega}\sum_{\nu,mn}\hat{\alpha}^{\nu\nu}_{mn}c^\dagger_{\nu m}c_{\nu n}\Big) \tag{C11}$$

we can obtain the effective single-particle Hamiltonian in the main text. The onsite atom-atom interaction $H_I = -U\sum_n c^\dagger_{sn}c^\dagger_{pn}c_{pn}c_{sn} = -U\sum_n n_{sn}n_{pn}$ is expressed as

$$H'_I = U(t)H_I U^{-1}(t) = H_I + H^{(1)}_I + \mathcal{O}(\frac{1}{\omega^2}), \tag{C12}$$

$$H^{(1)}_I = -g\frac{e^{i2\omega t} - 1}{2\hbar\omega}\Big[\sum_{mn}\Big(\hat{\alpha}^{ss}_{mn}n_{pn}c^\dagger_{sm}c_{sn} + \hat{\alpha}^{pp}_{mn}n_{sn}c^\dagger_{pm}c_{pn}\Big) - \sum_{\nu,n}\hat{\alpha}^{\nu\nu}_{nn}n_{sn}n_{pn}\Big] \tag{C13}$$

Items with $m = n$ in the first order correction $H^{(1)}_I$ vanish hence have no influence on the interactions. Items with $m = n \pm 1$ in $H^{(1)}_I$ modify the interactions to some kind of tunnelings terms which should be small. And considering that $1/\omega$ is also small, therefore in our calculations, it is a good approximation to assume that the interactions have the same form as that in a time-independent system.

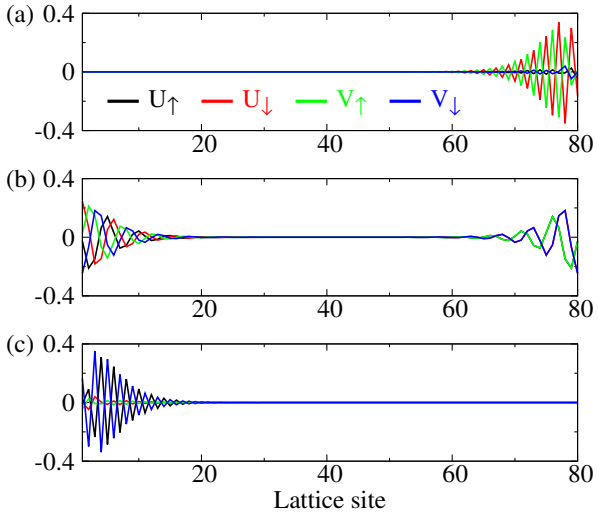

FIG. 8. (Color online) Wave functions of three pairs of edge states in real space. (a,b,c) are the wave functions of the three pairs of sub-gap edge states as shown in Fig. 4 of the main text for energy level E_n where $n = 80, 160, 240$. (a,c) are the wave functions closely related to the topological insulator when there are no interactions; (b) are the wave functions of zero-energy Majorana fermions. Other parameters are $\alpha = 1.4t_s$, $\mu = -1.0t_s$, $h = 0.8t_s$, $U = 4.0t_s$.

Appendix D: FFLO superfluids in a 2D shaken optical lattice

The FFLO superfluids induced by the shaken optical lattice also exist in a 2D case. For simplicity, we consider the one-photon coupling Ω between the lowest two orbital states and assume the Cooper pairing can only have a nonzero momentum along x direction. In the basis of $(\psi_{p_x}(\boldsymbol{k}_1), \psi_s(\boldsymbol{k}_1), \psi_s^\dagger(\boldsymbol{k}_2), -\psi_{p_x}^\dagger(\boldsymbol{k}_2))^T$ with $\boldsymbol{k}_1 = (Q/2 + k_x, k_y)$ and $\boldsymbol{k}_2 = (Q/2 - k_x, -k_y)$, the Hamiltonian reads

$$\mathcal{H} = \begin{pmatrix} \varepsilon_{p_x}(\boldsymbol{k}_1) & \Omega & \Delta & 0 \\ \Omega & \varepsilon_s(\boldsymbol{k}_1) & 0 & \Delta \\ \Delta & 0 & -\varepsilon_s(\boldsymbol{k}_2) & \Omega \\ 0 & \Delta & \Omega & -\varepsilon_{p_x}(\boldsymbol{k}_2) \end{pmatrix} \tag{D1}$$

where $\varepsilon_{p_x}(\boldsymbol{k}) = -t_p \cos(k_x a) + t_s^\perp \cos(k_y a) - \mu$ and $\varepsilon_s(\boldsymbol{k}) = t_s \cos(k_x a) + t_s^\perp \cos(k_y a) - \mu$. The phase diagram is shown in Fig. 7.

Appendix E: Coexistence of edge states in the shaken optical lattice

Without interaction, the system supports gap states which are localized on the system boundaries; When the interaction is turned on and the chemical potential cuts either the conduction or valance band, the system may support multiple edge states as shown in Fig. 8. The coexistence of the reminiscent edge states from topological insulator and the MFs edge states from topological superconductor may lead to many interesting transport properties in this system.

[1] I. Bloch, J. Dalibard and S. Nascimbène, Nat. Phys. **8**, 267 (2012).
[2] D. Jaksch, C. Bruder, J. I. Cirac, C. W. Gardiner, and P. Zoller, Phys. Rev. Lett. **81**, 3108 (1998).
[3] I. Bloch, J. Dalibard, and W. Zwerger, Rev. Mod. Phys. **80**, 885 (2008).
[4] M. Greiner, O. Mandel, T. Esslinger, T. W. Hänsch and I. Bloch, Nature **415**, 39 (2002)
[5] W. V. Liu and C. Wu, Phys. Rev. A **74**, 013607 (2006).
[6] C. Wu, Phys. Rev. Lett. **100**, 200406 (2008).
[7] M. Zhang, H.-h. Hung, C. Zhang, and C. Wu, Phys. Rev. A **83**, 023615 (2011).
[8] Y. Xu, Z. Chen, H. Xiong, W. V. Liu, and B. Wu, Phys. Rev. A **87**, 013635 (2013).
[9] G. Wirth, M. Ölschläger and A. Hemmerich, Nat. Phys. **7**, 147 (2011).
[10] P. Soltan-Panahi, D.-S. Lühmann, J. Struck, P. Windpassinger and K. Sengstock, Nat. Phys. **8**, 71 (2012).
[11] C. V. Parker, L.-C. Ha and C. Chin, Nat. Phys. **9**, 769 (2013).
[12] S. Choudhury and E. J. Mueller, Phys. Rev. A **90**, 013621 (2014).
[13] L.-K. Lim, C. M. Smith, and A. Hemmerich, Phys. Rev. Lett. **100**, 130402 (2008).
[14] P. Hauke, *et al.*, Phys. Rev. Lett. **109**, 145301 (2012).
[15] G. Jotzu, *et al.*, Nature **515**, 237-240 (2014)
[16] P. Fulde and R. A. Ferrell, Phys. Rev. **135**, 550 (1964).
[17] A. I. Larkin, and Y. N. Ovchinnikov, Zh. Eksp. Teor. Fiz. **47**, 1136 (1964).
[18] Y. Liao, A. S. C. Rittner, T. Paprotta, W. Li, G. B. Partridge, R. G. Hulet, S. K. Baur, and E. J. Mueller, Nature **467**, 567 (2010).
[19] X.-J. Liu, H. Hu, and P. D. Drummond, Phys. Rev. A **76**, 043605 (2007).
[20] M. M. Parish, S. K. Baur, E. J. Mueller, and D. A. Huse, Phys. Rev. Lett. **99**, 250403 (2007).
[21] Z. Zheng, M. Gong, X. Zou, C. Zhang, and G. Guo, Phys. Rev. A **87**, 031602(R) (2013).
[22] F. Wu, G. Guo, W. Zhang, and W. Yi, Phys. Rev. Lett. **110**, 110401 (2013).
[23] C. Qu, *et al.*, Nat. Commun. **4**, 2710 (2013).
[24] W. Zhang, and W. Yi, Nat. Commun. **4**, 2711 (2013).
[25] X.-J. Liu, and H. Hu, Phys. Rev. A **88**, 023622 (2013).
[26] C. Chen, Phys. Rev. Lett. **111**, 235302 (2013).
[27] Y.-J. Lin, K. Jiménez-García and I. B. Spielman, Nature **471**, 83 (2011).
[28] J.-Y. Zhang, *et al.*, Phys. Rev. Lett. **109**, 115301 (2012).
[29] C. Qu, C. Hamner, M. Gong, C. Zhang, and P. Engels, Phys. Rev. A **88**, 021604(R) (2013).
[30] P. Wang, *et al.*, Phys. Rev. Lett. **109**, 095301 (2012).
[31] L. W. Cheuk, *et al.*, Phys. Rev. Lett. **109**, 095302 (2012).
[32] M. Z. Hasan, and C. L. Kane, Rev. Mod. Phys. **82** 3045 (2010).
[33] X. L. Qi, and S. C. Zhang, Rev. Mod. Phys. **83** 1057 (2011).
[34] C. Zhang, S. Tewari, R. M. Lutchyn, and S. Das Sarma, Phys. Rev. Lett. **101**, 160401 (2008).
[35] M. Sato, Y. Takahashi, and S. Fujimoto, Phys. Rev. Lett. **103**, 020401 (2009).
[36] L. Fu, and C. L. Kane, Phys. Rev. Lett. **100,** 096407 (2008).
[37] S. Zhang, and Q. Zhou, Phys. Rev. A **90**, 051601 (2014).
[38] A. Schnyder, S. Ryu, A. Furusaki, and A. W. W. Ludwig, Phys. Rev. B **78**, 195125 (2008).
[39] A. Kitaev, AIP Conf. Proc. **1134**, 22-30 (2009).
[40] X.-J. Liu, K. T. Law, and T. K. Ng, Phys. Rev. Lett. **112**, 086401 (2014).
[41] J. He., *et al.*, Nat. Commun. **5**, 3232 (2014).
[42] X.-J. Liu, Z.-X. Liu, and M. Cheng, Phys. Rev. Lett. **110**, 076401 (2013).
[43] X. Li, E. Zhao, and W. V. Liu, Nat. Commun. **4**, 1523 (2013).
[44] W. Zhang, and H. Zhai, Phys. Rev. A **89**, 061603(R) (2014).
[45] M. König, *et al.*, J. Phys. Soc. Jpn. **77**, 031007 (2008).
[46] Y. Ohashi, and A. Griffin, Phys. Rev. Lett. **89**, 130402 (2002).
[47] E. Zhao, and A. Paramekanti, Phys. Rev. Lett. **97**, 230404 (2006).

[48] D. Wang, Z. Huang, and C. Wu, Phys. Rev. B **89**, 174510 (2014).
[49] E. Dumitrescu and S. Tewari, Phys. Rev. B **88**, 220505(R) (2013).
[50] C. Qu, M. Gong, Y. Xu, S. Tewari, and C. Zhang, arXiv:1310.7557.
[51] Z. Zheng, C. Qu, X. Zou, C. Zhang, arXiv:1501.00448.
[52] C. J. Wu, and S. Das Sarma, Phys. Rev. B **77**, 235107 (2008).
[53] K. Aikawa, A. Frisch, M. Mark, S. Baier, A. Rietzler, R. Grimm, and F. Ferlaino, Phys. Rev. Lett. **108**, 210401 (2012).
[54] M. Lu, N. Q. Burdick, S.-H. Youn, and B. L. Lev, Phys. Rev. Lett. **107**, 190401 (2011).
[55] M. Lu, N. Q. Burdick, and B. L. Lev, Phys. Rev. Lett. **108**, 215301 (2012).
[56] K. Aikawa, A. Frisch, M. Mark, S. Baier, R. Grimm, and F. Ferlaino, Phys. Rev. Lett. **112**, 010404 (2014).
[57] Y. Xu, R.-L. Chu, and C. Zhang, Phys. Rev. Lett. **112**, 136402 (2014).
[58] X.-J. Liu and H. Hu, Phys. Rev. A **85**, 033622 (2012).
[59] X.-J. Liu, L. Jiang, H. Pu, H. Hu Phys. Rev. A **85**, 021603(R) (2012).
[60] W. Zheng, B. Liu, J. Miao, C. Chin, and H. Zhai, Phys. Rev. Lett. **113**, 155303 (2014).
[61] S. Zhang, and Q. Zhou, Phys. Rev. A **90**, 051601 (2014).